View metadata, citation and similar papers at core.ac.uk

brought to you by CORE

provided by IntechOpen

We are IntechOpen, the world's leading publisher of Open Access books Built by scientists, for scientists

4,800
Open access books available

122,000
International authors and editors

135M
Downloads

Our authors are among the

154
Countries delivered to

TOP 1%
most cited scientists

12.2%
Contributors from top 500 universities

CLARIVATE ANALYTICS BOOK CITATION INDEX INDEXED

WEB OF SCIENCE™

Selection of our books indexed in the Book Citation Index in Web of Science™ Core Collection (BKCI)

Interested in publishing with us?
Contact book.department@intechopen.com

Numbers displayed above are based on latest data collected.
For more information visit www.intechopen.com

2

Internal Radiation Dosimetry: Models and Applications

Ernesto Amato, Alfredo Campennì, Astrid Herberg,
Fabio Minutoli and Sergio Baldari
University of Messina, Department of Radiological Sciences,
Nuclear Medicine Unit,
Italy

1. Introduction

Internal radiation dosimetry has a fundamental and growing role in planning nuclear medicine therapies with radionuclides.

The principle of nuclear medicine therapy is to destroy pathologic tissues through the irradiation with the ionizing radiation emitted by properly chosen radionuclides, while preserving other organs and tissues from unnecessary exposure to the same radiation.

In order to realize this result, proper pharmaceuticals are chosen with a biodistribution targeted on target tissues, and labelled with a suitably chosen radionuclide. The choice of the best radionuclide is carried on with the aim of maximizing radiation energy deposition in the target tissue during the desired treatment time. Beta-emitters are the best choice in most cases, because beta radiation has a mean range in tissue from few millimetres to few centimetres. Also used are alpha- and Auger-emitters, for millimetre and sub-millimetre ranges.

The absorbed dose to the target tissues as well as to other organs and tissues depends from the biokinetics of the radiopharmaceutical and from the physical decay scheme of the radionuclide employed. While the physical properties of each nuclide are well known from experimental data, the biodistribution of the radiopharmaceutical within the patient's body depends on the dynamic biologic pathway that in turns is governed by the role of the molecule, by the characteristics of the patient, by the type and stage of the disease, and by the route of administration.

The distribution of radioactivity within the human body must be sampled several times post-administration, by means of planar or tomographic (SPECT or PET) imaging techniques. Tomographic techniques are rapidly substituting planar whole body imaging, since, thanks also to the accurate attenuation correction and image co-registration brought by a simultaneous CT scan, they reach a spatial resolution and an accuracy in activity quantification unprecedented.

After a general introduction on dosimetric quantities and their relationships, we focus on the dosimetric anthropomorphic models. We introduce also 3D techniques based on voxel dose factors, convolution of dose point-kernels and direct Monte Carlo computation, focusing on the contribution of Monte Carlo simulation to the development of new and more accurate dosimetric and microdosimetric models for internal dosimetry.

We describe the application of such dosimetric approaches in the main nuclear medicine therapies such as the ^{131}I therapy of thyroid diseases, the therapy of neuroendocrine tumours (NET) with somatostatin analogues labelled with beta- or Auger-emitters, and the palliation of painful bone metastases, focusing on dose-efficacy relationships and on the limiting of side effects to other potentially critical organs.

2. Definitions

If we consider a radioactive volume containing, at the time t, N radioactive nuclei, we know that the activity $A(t)$, representing the number of decays per second, is proportional to N through the decay constant λ:

$$A(t) = \frac{dN}{dt} = -\lambda N \tag{1}$$

Equation 1 can be integrated, leading to the exponential decay law for the number of radio-atoms present at the time t in a radioactive sample:

$$N = N_0 e^{-\lambda t} \tag{2}$$

The decay constant λ is related to the decay time τ and to the half-life $T_{1/2}$ by the relationships:

$$T_{1/2} = \frac{\ln 2}{\lambda} = \tau \ln 2 \tag{3}$$

The SI unit of activity is the *Becquerel* (Bq), defined as one disintegration per second:

$$1Bq = 1dis \cdot s^{-1}\ , \tag{4}$$

while the old unit of activity was the *Curie* (Ci):

$$1Ci = 3.7 \times 10^{10} Bq \tag{5}$$

The radiation absorbed dose, commonly intended as dose, is defined as the average energy imparted by the radiation per unit mass of the irradiated volume:

$$D = \frac{d\bar{E}}{dm} \tag{6}$$

In the SI system, the dose is expressed in joules per kilogram or Gray (Gy); the older unit, no longer employed but often encountered in aged texts, was the Rad (1 erg/g). The conversion is such that 1 Gy = 100 Rad.

In internal dosimetry, the dose to an organ or tissue accumulating a radiopharmaceutical can be evaluated following the MIRD approach (Snyder et al., 1975).

The dose imparted to a target volume k from a single source volume h, can be calculated as:

$$D(r_k \leftarrow r_h) = \tilde{A}_h S(r_k \leftarrow r_h) \tag{7}$$

where $\tilde{A}_h$ is the cumulated activity in the source organ and S is the average dose absorbed by the target per unit cumulated activity in the source. The cumulated activity in h is defined as the total number of disintegrations in that organ, i.e. the integral of the activity A over the time:

$$\tilde{A}_h = \int_0^\infty A_h(t)dt \ , \tag{8}$$

The definition of the S factor appearing in Equation 7 is:

$$S(r_k \leftarrow r_h) = \frac{\sum_i \Delta_i \varphi_i (r_k \leftarrow r_h)}{m_k} \tag{9}$$

where Δ_i is the average energy emitted per transition as i-th radiation, φ_i is the "absorbed fraction", i.e. the fraction of the energy emitted in the source volume r_h which was absorbed in the target volume r_k, and m_k is the mass of the target.
In general, if several organs accumulate the radiopharmaceutical, the overall dose to the target volume (organ or tissue) k is obtained by summing up all the contributions coming from the various regions h:

$$D(r_k) = \sum_h \tilde{A}_h \sum_i \Delta_i \Phi_i (r_k \leftarrow r_h) / m_h \tag{10}$$

Another usually employed quantity is the residence time, defined as the ratio between the cumulated activity in h and the administered activity A_0:

$$\tau_h = \frac{\tilde{A}_h}{A_0} \tag{11}$$

Even if the residence time has the physical dimensions of a time and it is often indicated with the same Greek letter, it must not be confused with the decay time of a radionuclide. In fact, while the decay time is the time necessary to reduce by 1/e = 0.37 the activity of an isolated sample, the residence time is the length of time an activity A_0 would have to reside in the volume to give that cumulated activity.

3. Radiobiological models of the radiation effects

The estimation of the effect of the radiation absorbed dose in biological tissues can not neglect biological models accounting for the ability of tissues and cells to repair in some degree the radiation-induced injury. (Cremonesi, 2011; Strigari, 2011)
The radiation damage can vary due to the different tissue properties (the "five Rs" of radiobiology: *repair*, *repopulation*, *reoxigenation, redistribution* and *intrinsic radiosensitivity*) in tumours and in healthy tissues, and due to the difference in possible irradiation regimes (type and energy of the radiation, dose rate, repetition or fractionation of treatments).
In nuclear medicine therapies with radiopharmaceuticals, the radiation dose is often imparted by beta or Auger electrons, even if the role of alpha emitters as therapeutic agents is increasing again.

Thus, the dose and the dose rate in the single treatment are governed by the biokinetics of the radiopharmaceutical and by the administered activity and route of administration.
The biological effect of such irradiation in tumours and in healthy tissues will depend firstly on the *repair* ability of the sub-lethal damage with related repair time T_{rep}, which is due to the mechanisms that counteract all the natural damages to the DNA. This is the fastest mechanism influencing the response to irradiation, since its effects are detectable in external irradiations already after 30 minutes.
The cell life cycle is divided in four consecutive steps: G1, S, G2 and M. The two gaps of apparent inactivity, G1 and G2, divide the two active phases, the DNA synthesis S and the mitosis M. Radiobiology studies demonstrated that the highest cell radiosensitivity belongs to G2 and M phases. After an irradiation, the survival fraction will be higher for cells in the G1 or S phases; thus a *redistribution* of population is initiated, with a synchronization of cell life cycles.
This effect could, in principle, play a certain role in external irradiations repeated at the times of higher sensitivity, but no clear evidence of efficacy has been demonstrated yet.
Cells surviving to an exposure to radiations will continue to proliferate; such a repopulation has a detrimental effect on therapeutic results. On the other hand, tumour cell death leads to tumour tissue shrinkage and, consequently, can improve the *reoxigenation* of the residual hypoxic cells. Since hypoxic cells are more radio-resistant than the oxygenated ones, repeated cycles of irradiation are useful to improve therapeutic outcomes.
As a consequence of these mechanisms, the effect of a radiation therapy depends not only on the radiation absorbed dose, but also on the dose rate and on the fractionation regime.
The most widely applied radiobiological model describing cell survival after irradiations is the linear-quadratic model, in which the effect E, in logarithmic relation with the surviving fraction SF, is a function of the dose D and the dose squared:

$$E = -\log(SF) = \alpha D + \beta D^2 \tag{12}$$

The linear component accounts for the lethal cell damage given by a single radiation producing, for example, double-strand breaks of the DNA helix, while the quadratic component accounts for the lethal damage obtained by summing up the effects of two consecutive ionizing radiations. It should be noticed that the parameter α has dimensions of Gy^{-1}, while β of Gy^{-2}. The dose in correspondence of which the linear contribution L equals the quadratic one Q (see Fig. 1), is given by $D = \alpha/\beta$ (Gy). This value expresses the *intrinsic radiosensitivity* of the tissue, and external as well as internal radiation therapies exploit the higher radiosensitivity of cancer cells with respect to normal tissue cells.
When the radiation dose is imparted in a time T comparable or even longer than the repair time of the sub-lethal damage, T_{rep}, Eq. 12 must be corrected in order to account for the competition between radiation-induced damage and cell repair rate:

$$E = -\log(SF) = \alpha D + g(T)\beta D^2 \tag{13}$$

where $g(T)$ is a properly chosen function of the irradiation time. When $T >> T_{rep}$, as in the case of targeted radionuclide therapies, it was demonstrated that a good approximation is:

$$g = \frac{T_{rep}}{T_{rep} + T_{eff}} \tag{14}$$

where T_{eff} is the effective half-life of the radionuclide in the target tissue.

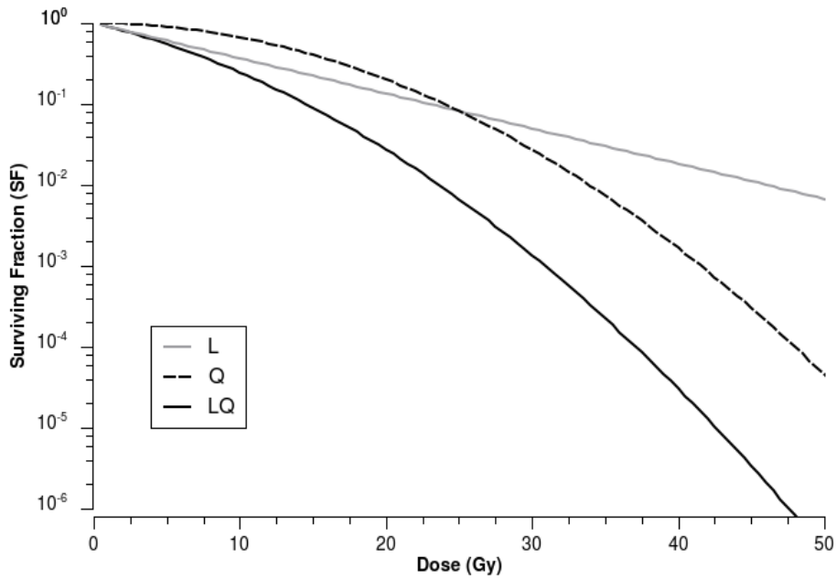

Fig. 1. Cell surviving fraction as a function of the radiation dose, following the linear-quadratic (LQ) model. Linear (L) and quadratic (Q) part of the equation are represented, too. In the proposed example, $\alpha/\beta = 25$ Gy.

The Biologically Effective Dose (*BED*) is defined in a way such that the effect *E* is linearly related to *BED* through the parameter α:

$$E = \alpha BED \tag{15}$$

From Eq. 13, *BED* is related to the cell surviving fraction and to the dose with the relationships:

$$BED = -\frac{1}{\alpha}\log(SF) = D + \frac{\beta}{\alpha}g(T)D^2 \tag{16}$$

For radionuclide therapies, Eq. 14 holds for the correction factor *g*, resulting, for a single irradiation imparting a radiation dose *D*:

$$BED = D + \frac{\beta}{\alpha}\frac{T_{rep}}{T_{rep}+T_{eff}}D^2 \tag{17}$$

In the case of repeated irradiations, each one imparting a dose D_i, the total *BED* can be calculated as:

$$BED = \sum D_i + \frac{\beta}{\alpha}\frac{T_{rep}}{T_{rep}+T_{eff}}\sum D_i^2 \tag{18}$$

In the next Sections, we will see how BED is related to the impairment of kidneys after repeated cycles of peptide radio-receptor therapies (PRRT) with somatostatin analogues

labelled with beta-emitting radioisotopes. In such evaluations, it is usually assumed α/β = 2.4 Gy and for T_{rep} a value of 2.8 hours.

4. Time sampling and determination of the cumulated activity

In Section 2, the main equations of internal dosimetry were introduced, and the role played by the cumulated activity, i.e. the total number of disintegrations in the considered target, was taken in evidence.

In general, the biokinetics of a radiopharmaceutical within the human body will be influenced by the type of the carrier molecule and its physiologic and pathologic pathway, by the route of administration and by the preparation and clinical state of the patient. Clinical studies and trials give information about the average residence times of groups of patients, but, in order to plan the single treatment, only an accurate individualized dosimetry can be usefully employed.

In order to calculate the cumulated activity, the activity up-taken in each organ or region of interest must be properly sampled after administration. In principle, more measurements allow a more accurate fit of the A=A(t) curve, and, consequently, a better estimation of the total number of disintegrations.

However, we must remember that each measurement is carried out through planar scintigraphic or emission computed tomography (ECT) techniques, which are time consuming for both patient and hospital personnel.

Even in the case of non-imaging techniques, such as thyroid uptake measurements with a scintillation probe, the patient must come back to the nuclear medicine department for each measurement.

Hence the need to optimize dosimetric protocols in order to the number and timing of the acquisitions. The optimal choice will depend on the expected biokinetics of the radiopharmaceutical in the organs of interest, which can be assumed from previous clinical studies.

The simplest model applies when the uptake phase, i.e. the phase in which the radiopharmaceutical is accumulating in the organ and its radioactivity rises with time, is short enough to be considered instantaneous. Consequently, immediately after administration, the washout phase begins.

If, in the simplest assumption, the radiopharmaceutical is washed out with a mono-exponential rate, the variation of N with time follows a law analogous to Eq. 1:

$$\frac{dN}{dt} = \lambda_{eff} N \tag{19}$$

where the effective decay constant $\lambda_{eff} = \lambda + \lambda_{bio}$ is given by the sum of the physical decay constant introduced in Eq. 1 and the biological decay constant, characteristic of the biological wash-out of the radiopharmaceutical from the organ. In analogy with Eq. 3, the effective decay time τ_{eff} and the effective half-life T_{eff} can be defined as:

$$T_{eff} = \frac{\ln 2}{\lambda_{eff}} = \tau_{eff} \ln 2 \tag{20}$$

and the cumulated activity will be:

$$\tilde{A} = A\int_0^{\infty} e^{-\lambda_{eff}t}\,dt = \frac{A}{\lambda_{eff}} \tag{21}$$

In more complex cases, the uptake phase can require a certain amount of time and, consequently, the assumption of instantaneous uptake must be released and the uptake phase can be usually described by an exponential growth. Furthermore, the washout phase can be not accurately described by a simple mono-exponential decay. For example, a bi-exponential curve can fit better to a biokinetical behaviour composed by a first phase of rapid clearance in which the biologic half-life is much smaller than the physical half-life, followed by a slower retention phase in which, on the contrary, it is the physical half-life that governs the overall effective half-life.

In Figure 2, an example of near-instantaneous uptake, followed by a washout phase described by a bi-exponential decay, is shown. The renal uptake of a diagnostic dose of ^{111}In-DTPA-Octreotide, a somatostatin analogue used for the diagnosis of neuroendocrine tumours, was imaged at 1, 6, 24 and 48 hours post-injection.

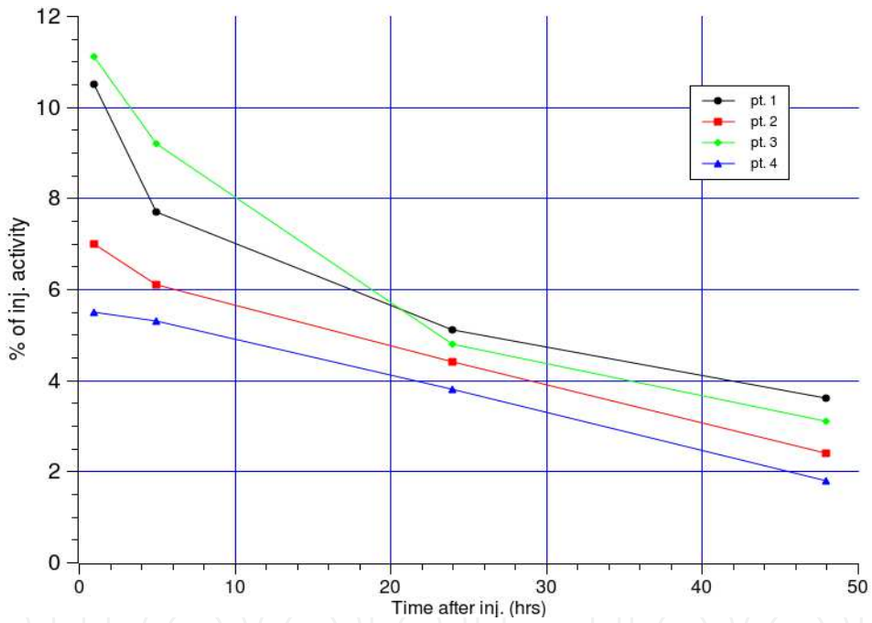

Fig. 2. Uptake curves for kidneys in four patients after ^{111}In-DTPA-Octreotide intravenous administration.

In Figure 3 we present three examples of ^{131}I uptake curves for hyperthyroid patients (pt. 1 and 2 affected by toxic nodular goitre, TNG, and the third by Basedow disease), acquired by means of a scintillation probe at six times after oral administration of a diagnostic activity of 1.8 MBq.

In these cases, the uptake phase is expected to last up to one day, followed by a decay phase with a characteristic half-life of 100-200 hours, deriving from both physical (eight days) and biological decay.

Thanks to the simplicity and rapidity of thyroid uptake measurements with a gamma probe, it is possible to sample properly in time these patients. Usually, two measurements during the first day, 3 and 6 hours after oral administration, properly characterize the uptake phase.

Measurements can proceed at 24, 48, 72 (or 96, or 120) and 168 hours, in order to detect the maximum uptake and the decay phase.
Points can be then fitted with the function:

$$U(t) = \frac{\lambda_{\text{in}} U_{max}}{\lambda_{\text{out}} - \lambda_{\text{in}}} \left(e^{-\lambda_{\text{in}} t} - e^{-\lambda_{\text{out}} t} \right) \tag{22}$$

where the uptake and washout constants λ_{in} and λ_{out} depend upon the rapidity of the increase and decrease in uptake, respectively.
Even if the maximum uptake is expected, on average, around 24 hours, this is not a rigid rule, of course. Patient 3, for example, reached the maximum uptake already at the sixth hour, and the fit of patient 1 data show its maximum earlier than 24 hours; cases of late maxima are observed, too.
In order to evaluate properly the effective half-time of the washout phase, measurements should extend at least up to 120 hours, better up to 168 hours. In fact, since each point is affected by statistical fluctuations and by minor biases due to the practical procedure, repeated measurements help in reducing errors in fit.
As an example, in Figure 3 we represent, together with the fits of the whole data series (solid lines), the fits obtained by considering only the first four points, i.e. 3, 6, 24 and 48 hours (dashed lines).
It is apparent from figure the underestimation of the decay time for the first patient, and, on the contrary, the overestimation for the second one.
Such outcome is confirmed numerically by the results reported in Table 1, where the effective half-time of the washout, T_{eff}, is calculated from the decay constants obtained from the complete fit and from the 3-48 hours data. Results from incomplete data give a 24% shorter half-time for the first patient, while for the second one an overestimation as high as 91% comes from a dosimetric protocol limited to 48 hours.

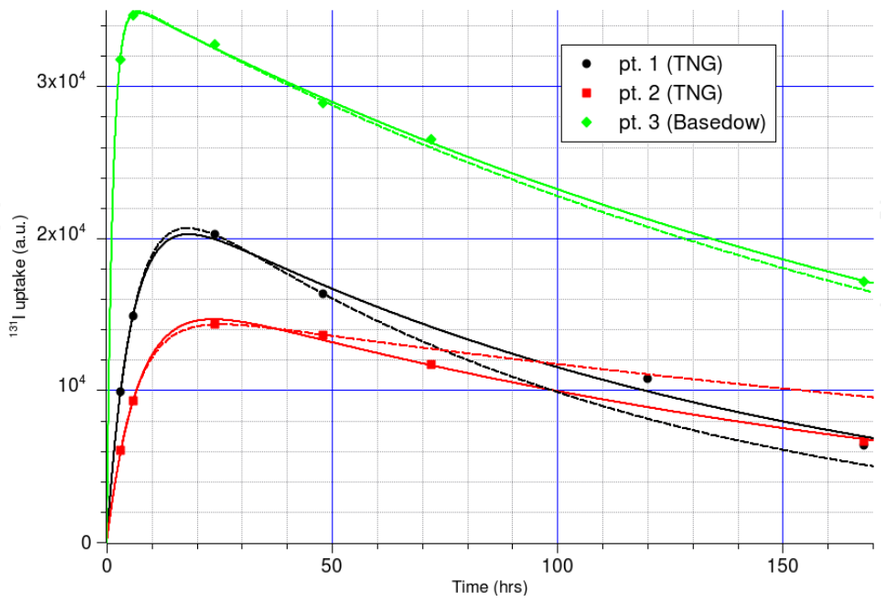

Fig. 3. ^{131}I uptake curves for the three patients. Solid curves represent the analytical fits of complete data series with Eq. 22, dashed lines represent fits of 3-48 hours data.

Pt. no.	U_{max}	λ_{in}	λ_{out}	λ_{out}(48h)	T_{eff}	T_{eff}(48h)	error
1 (TNG)	23184	0.184	7.41E-3	9.72E-3	93	71	-24%
2 (TNG)	16755	0.142	5.62E-3	2.95E-3	123	235	+91%
3 (Bas.)	35920	0.740	4.42E-3	4.66E-3	157	148	-6%

Table 1. Fit parameters for the complete data series, and for the first four points. Relative error in T_{eff} determination are reported.

5. Anthropomorphic models for internal dosimetry

In the past decades, several schematic anthropomorphic models were proposed in order to standardize and simplify dose calculation both in medical applications of radionuclides and in internal contamination evaluations for radiological protection purposes.
Among these, a common approach to internal dosimetry is based on standardized phantoms and S factors pre-calculated for couples of Source-Target organs and for various radionuclides (Snyder et al., 1975).
Organ S factors were calculated through Monte Carlo simulations and are currently available in a tabular form. As a consequence, once calculated the cumulated activity in the source organ with the methods described in the previous Section, the dose to the target organ is calculated with Equation 7, using the proper S factor accounting for the radionuclide emission and for the geometry of the source-target couple.
An advantage of this method is the simplicity of measurements and the standardization of the dosimetric procedure, allowing easier comparisons between results. However, the simplified organ models, described by fixed geometrical shapes and volumes, do not account properly for the anatomy of the single patient. Furthermore, each organ is treated as a whole, neglecting inhomogeneity in the uptake within each organ or tissue.
In real cases, the shape and size of an organ can be varied by a disease, and pathologic tissues, which are the target of the treatment, are not present in standard models of healthy humans.
A sphere model is often employed in order to represent small target tissues such as tumours or pathologic lymph-nodes. Recently, we developed a model to calculate the absorbed fractions in ellipsoidal shapes uptaking beta-gamma emitting radionuclides (Amato et al. 2009, 2011).
Considering a radionuclide which emits mono-energetic and beta electrons, and gamma photons, the average dose to the target volume is given by:

$$\overline{D} = D_\beta + D_e + D_\gamma = \frac{\tilde{A}}{m}\left[\int \frac{dn(E)}{dE} E\varphi(E)\,dE + \sum_i \left(n_{e,i}E_{e,i}\varphi_{e,i} + n_{\gamma,i}E_{\gamma,i}\varphi_{\gamma,i}\right)\right], \tag{23}$$

where n_e and n_γ are the mono-energetic electron and gamma photon emission probabilities, respectively, of energies E_e and $E\gamma$, φ_e and φ_γ are the electron and photon absorbed fractions. These absorbed fractions can be derived from the equation:

$$\varphi(\rho) = \left(1 + \frac{\rho_0}{\rho^s}\right)^{-1} \tag{24}$$

where ρ is the "generalized radius", defined as:

$$\rho = 3\frac{V}{S} \tag{25}$$

where V and S are the volume and surface of the ellipsoid. The parameters ρ_0 and s in Equation 24 depend on the nature (electron or photon) and energy of the radiation, and can be derived from proper parametric functions described in (Amato et al. 2009, 2011).
In Figure 4, the absorbed fraction as a function of the generalized radius is reported for photons and electrons uniformly emitted in ellipsoids of various shapes. These data are calculated by means of a Monte Carlo simulation in Geant4.

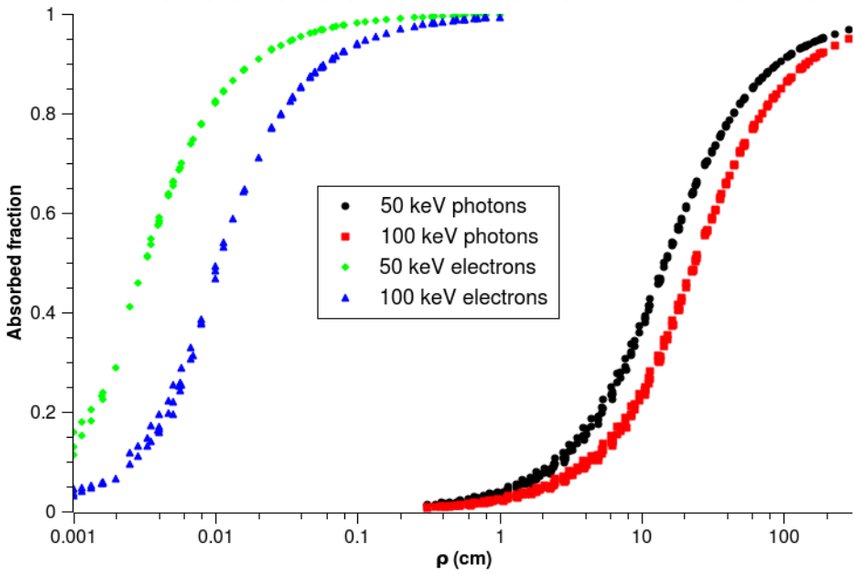

Fig. 4. Electron and photon absorbed fraction in ellipsoidal volumes, as a function of the generalized radius (Amato et al. 2009, 2011).

6. Three-dimensional dosimetry

Traditional approaches to internal dosimetry employ anatomic models to obtain mean organ doses. With the diffusion of SPECT-CT and PET-CT tomographs, dosimetric methods which can utilize non-uniform activity distributions to derive dose distributions within organs become increasingly important.
This result can be obtained either with dose point-kernel convolution methods, or by means of a direct Monte Carlo simulation, or exploiting the voxel S factor approach.
The voxel S factor approach, introduced in (Bolch et al., 1999), has been used more widely than dose point-kernel and direct Monte Carlo computation approaches, due to its recognized simplicity.
Following this approach, the average dose to the k-th voxel can be calculated as:

$$\bar{D}_k = \sum \tilde{A}_h \cdot S_{k \leftarrow h} \tag{26}$$

where $\tilde{A}_h$ is the cumulated activity in the generic h-th voxel and $S_{k \leftarrow h}$ is the voxel S factor, defined as:

$$S_{k\leftarrow h} = \sum \Delta_i \cdot \frac{\varphi_i(k \leftarrow h)}{m_k} \tag{27}$$

where Δ_i is the mean energy emitted as radiation i per decay, φ_i is the absorbed fraction in k of the radiation i emitted in h, and m_k is the mass of the k-th voxel.

In (Bolch et al., 1999), voxel S factors were tabulated for five radionuclides and two cubic voxel sizes. Recently, Dieudonnè et al. (2010) presented a generalization of this approach to variable voxel sizes, which allows to obtain S factors for a generic voxel size for nine radionuclides by means of a resampling method.

The dose point-kernel gives the dose per decay event at a given distance from a point source located inside an infinite and homogeneous absorbing medium. Dose point-kernels for electrons and photons were calculated by means of Monte Carlo simulations, and are available either in tabular form or as analytical functions obtained fitting the simulative data (Mainegra-Hing et al., 2005) (Maigne et al., 2011).

By convolving the dose point-kernels evaluated for the actual radionuclide spectrum in the three-dimensional distribution obtained from the volume distribution of cumulated activity, obtained from SPECT-CT or PET-CT images, one can retrieve the volume distribution of the absorbed dose. In order to speed up calculations, fast Fourier or fast Hartley transformations can be employed.

Finally, the Monte Carlo approach is the most demanding in terms of computational power, but it is the only one which can account accurately for tissue inhomogeneity. Known the three-dimensional map of tissue density and composition from CT scan and the volume distribution of the cumulated activity through SPECT or PET emission tomography, it is possible to generate a fixed number of decay events statistically distributed in space according to emission tomography data within the patient's body reconstructed from CT and track all the emitted secondaries in order to calculate the geometrical distribution of energy deposition, i.e. the three-dimensional map of absorbed dose, and finally to rescale the results to the actual values of cumulated activity (Furhang et al., 1997).

7. ^{131}I therapy of hyperthyroidism

Hyperthyroidism is a consequence of an excess in free-thyroid hormone action on the tissues. The most frequent causes of hyperthyroidism are: Graves' Disease (GD), Toxic Adenoma (TA) or Toxic Multinodular Goiter (TMG). In any cases, hyperthyroidism can be caused by sub-acute thyroiditis or silent thyroiditis.

The treatment of GD, TA and TMG can be symptomatic with anti-thyroid drugs (often used as first line therapy) or definitive: radioiodine therapy (RaIT) or surgery (total or near-total thyroidectomy).

RaIT is a well established method for the treatment of hyperthyroidism; aim of the RaIT is to achieve an euthyroid or hypothyroid (such as in the Graves patients) status.

Presently, the optimal ^{131}I activity to be administered is still matter of debate.

Many authors evaluated the effectiveness of different dosimetric methodologies. The results were variable and often controversial, in order to the frequency of recurrence and hypothyroidism (Regalbuto et al., 2009) (Giovannella, 2000).

In order to determine the ^{131}I activity to be administered for the treatment of hyperthyroidism, fixed activity and adjusted activity approaches are currently employed. In

both cases it is necessary, if possible, to suspend anti-thyroid drugs treatment 4-6 days before RaIT or thyroid scintigraphy.
The ^{131}I "fixed"activity for RaIT is usually about 555 MBq. In such case, the thyroid scintigraphy with or without radioiodine thyroid uptake (RTU) curve can be not necessary.
In the adjusted activity approach, a dosimetric procedure is employed which requires two diagnostic steps: a) thyroid ultrasonography to calculate the volume of the gland, or the hot thyroid nodule(s), assuming for them an ellipsoidal shape; b) thyroid scintigraphy and RTU measurements after ^{131}I tracer activity administration (1.8 MBq).
The dosimetric method most frequently employed was proposed by the MIRD commission (Snyder et al., 1975). In this approach, RTU measurements are usually conducted between 3 and 120 hours after administration. Multiple RTU measurements allow to calculate the effective half-life of the radioiodine into the hot nodules or in the whole gland (Figure 3).
In TMG and TA patients, the effective volume of the hot nodule(s) was calculated taking into account the presence of involving area(s) (whole nodule volume - involving area volume).
The radiation doses to be imparted to the gland (GD) or to the nodule(s) (TA and TMG) are up to 200 and 300 Gy, respectively.
In GD with ophtalmopathy, the radiation dose to be imparted must be adjusted, up to a maximum value of 250 Gy. In these patients, it is useful to administer anti-inflammatory drugs for a time duration ranging from 4 to 12 weeks after RaIT.
In all patients, the choice of the therapeutic dose will be determined also in function of: sex and age, type of hyperthyroidism (overt or sub-clinical) and its temporal duration, concomitant Hashimoto thyroiditis, anti-thyroid drugs therapy and its temporal duration.
Basing on the above considerations, the activity to be administered can be calculated as:

$$A = 5.829 \frac{Dm}{U_{max} T_{1/2eff}} \tag{28}$$

where A is the activity to be administered in MBq in order to impart a dose D in cGy to the target (nodule or gland) of mass m in g, U_{max} is the maximum per cent radioiodine uptake (usually measured at 24 hours) and $T_{1/2eff}$ is the effective half-time in hours.
Recently, Amato et al. (2011) proposed an improved calculation method for the activity to be administered during the radioiodine treatment of hyperthyroidism. In this approach, a Monte Carlo simulation had been employed to derive the radiation dose in nodules or in the whole gland within an anthropomorphic phantom, taking into account the ellipsoidal shape of the target volumes.
As a result, the activity to be administered can be calculated with the formula:

$$A = \frac{Dm}{U_{max} T_{1/2eff}} \cdot \frac{32.31\rho + 1}{\rho\left(0.2625\rho + 5.1819\right)} \tag{29}$$

where we recall the definition of generalized radius, $\rho = 3V/S$, stated in Equation 12, and here expressed in cm. The volume and the surface of the ellipsoidal target (nodule or thyroid lobe) can be calculated from the semiaxes measured through ultrasonography as:

$$V = \frac{4}{3}\pi abc\,, \qquad S = 4\pi \left(\frac{(ab)^p + (bc)^p + (ac)^p}{3} \right)^{1/p} \tag{30}$$

8. ^{131}I therapy of differentiated thyroid carcinoma

Differentiated thyroid cancer (DTC) is the most common cancer of the endocrine system.
The first line therapy is represented by total or near-total thyroidectomy (with dissect of the sixth lymph nodes level and, if necessary, of the lateral-cervical lymph nodes of the same side respect to primary lesion).
After Total or near-Total Thyroidectomy (nTT) it is useful to ablate the thyroid remnant with 131-radioiodine therapy (RaIT). In fact, several Authors, such as Mazzaferri et al. (1997) demonstrated that the *prognosis quod vitam* and the survival curve of the DTC-patients significantly improve if RaIT follows TT or NTT.
In addition, the ablation of thyroid remnant (TRA) allows a better management of the follow-up of these patients.
In fact, in the patients treated with TT or NTT and TRA, the Thyroglobulin (hTg) serum levels should be undetectable. Thus, any enhancement of hTg serum (both under L-T4 suppressive therapy or after exogenous TSH stimulation -rhTSH-) can be considered as a relapse of disease.
RaIT can be carried out in hypothyroidism state (TSH>=30) or after rhTSH stimulation.
Post dose whole body scan and static images of the head, neck and thorax acquired 4-8 days after RIT allow to identify the thyroid remnant and metastases (loco-regional and/or distant).
For the RaIT of TRA, fixed activities are employed more frequently: 1110, 2220 or 3700 MBq.
In the patients treated after rhTSH stimulation it is necessary to employ a medium-to-high activity of radioiodine (2220 and 3700 MBq, respectively), because in this condition the effective half-life of radioiodine in the thyroid remnant is shorter than in the state of hypothyroidism.
However, the TRA activity can be adjusted through a dosimetric approach (Lassmann, 2010), which requires a pre-therapeutic scintigraphy with ^{131}I or ^{124}I PET. The dose to the thyroid remnant can be calculated using ^{131}I post-therapy whole body scan, too.
Both methods show advantages and disadvantages. The main disadvantage of the pre-therapeutic scintigraphic method is correlated to the stunning or mass change effects that could be determined by a diagnostic activity of ^{131}I.
On the other hand, the main disadvantage of the post-therapeutic scintigraphic method is correlated to technical difficulties such as the limitations deriving from the gamma-camera dead time.
The clinical evidence demonstrated that the dosimetry adjusted activities do not differ significantly from the fixed values. Thus, in the clinical practice, the dosimetric approach is not employed frequently. However, the dosimetric approach is useful for the treatment of loco-regional and/or distant metastases.
Dosimetry is particularly useful in patients with lung and/or bone metastases, where standard activities can lead to a radiation dose imparted to the lesions lower than the necessary. In such cases, it is necessary to acquire some whole scans starting from 6-7 hours after radio-iodine therapy. (Eschmann et al., 2002) (Sgouros et al., 2004).

9. Usefulness of radiopharmaceuticals for the palliation of painful bone metastases

The development of bone metastases is commonly related to a serious reduction in quality of patient life because of pain occurrence and side effects of analgesics intake, especially

opiates (Silberstein, 2001). Therapeutic options for pain palliation include systemic therapy with cytotoxic agents, diphosphonate therapy, external beam radiotherapy and radionuclide therapy. Diphosphonate therapy has become a possible option for the treatment of patients affected by bone metastases since a new generation of diphosphonate has been developed; using zoledronic acid, indeed, the clinical benefits of diphosphonate (skeletal complications reduction and analgesic effects on bone pain), previously limited to patients with bone metastases from breast cancer or lesions due to multiple myeloma, have been extended to patients with bone metastases secondary to a broad range of solid tumors (Berenson, 2005). However, diphosphonates achieve only a modest analgesic effect and are associated with some non-renal adverse effects (Hillner, 2003; Lewington, 1996). External beam radiotherapy is the therapy of choice in cases of a single site of pain. However, when multiple painful metastases have been developed, local field radiotherapy is less effective and hemibody radiotherapy is associated with a significant morbidity (Lewington, 1996). Furthermore, external beam radiotherapy is often not suitable for repeated treatments. On the other hand, bone-seeking beta-emitting radiopharmaceuticals represent an effective tool for pain palliation in patients with multifocal bone disease, and make it possible to perform multiple administrations (Lam, 2004; Daformou, 2001; Englaro, 1992; Maini, 2003). Pain arises from both umoral and mechanical effects, including bone invasion, micro-fractures, increased intramedullary pressure and periosteal stretching (Lewington, 2005). Unlike opiates, which affect the entire nervous system, radionuclides exert their action mainly on cells at the peripheral nerve endings, where inflammatory, immune and malignant cells accumulate and release chemicals that modulate pain at the site of malignant invasion (Krishnamurthy, 2000). Furthermore, early response gene induction and a psychological-placebo component could account for the pain alleviation effect (Lewington, 1996; Leondi, 2004; Roche, 1994; Hellmann, 1994).

The goals of therapy are to alleviate pain, improve quality of life and mobility, reduce dependence on narcotic and non-narcotic analgesics, and improve performance status and possibly survival (Minutoli, 2006; Hindorf, 2011).

Bone tumours can be divided into osteolytic and sclerotic tumours. Sclerotic tumours are more suitable for targeted radionuclide therapy because of higher uptake of the radiopharmaceutical within the lesions. The majority of bone metastases from prostate cancer are sclerotic whilst metastases of breast cancer generally are mixed osteolytic/sclerotic. Also patients with bone metastases from tumours other than prostate and breast cancer and increased ^{99m}Tc-MDP uptake on bone scan can benefit from targeted radionuclide therapy (Leondi, 2004; Minutoli, 2006).

Two radiopharmaceuticals for the treatment of bone tumours are currently approved by the European Medicines Agency (EMEA): ^{153}Sm-EDTMP (Quadramet®) and ^{89}Sr-Cl_2 (Metastron®). Other radiopharmaceuticals are at different stages of research, or are approved in some European Countries. These include ^{186}Re-HEDP, ^{117m}Sn-DTPA and ^{223}Ra-Cl_2 (Alpharadin®). The use of ^{32}P is now considered to be obsolete.

Strontium-89 was suggested for the treatment of bone tumours during the 1940s. It is naturally taken up in bone and is a pure β^- emitter with a long half-life (50.53 days). Pharmacokinetic and dosimetry studies have been based on imaging of ^{85}Sr-Cl (Blake, 1986, 1987, 1998; Breen, 1992), although imaging based on bremsstrahlung photons from ^{89}Sr has also been performed (ICRP, 1997). Tumour dosimetry is generally performed under the assumption that the activity uptake is five times higher than for normal bone. Strontium

leaves the blood quickly after an intravenous injection. The kidneys are the main route of excretion, but the gut has been seen in scintillation camera images and IRCP report assumes 4:1 ratio for urinary to faecal excretion.

Tin-117m labelled DTPA is investigated for the treatment of bone pain from metastases. Tin-117m can be imaged via the 156 keV gamma photons and the main energy deposition is performed by the corresponding conversion electrons. The conclusion from a phase I/II clinical study was that ^{117m}Sn-DTPA is an effective and safe radiopharmaceutical for the treatment of bone metastases (Krishnamurthy, 1997; Srivastava, 1998).

^{153}Sm-EDTMP is a therapeutic agent consisting of radioactive samarium and a tetraphosphonate chelator, ethylenediaminetetramethylenephosphonic acid (EDTMP). It is formulated as a sterile, non-pyrogenic, clear, colorless to light amber isotonic solution of samarium-153 lexidronam for intravenous administration (37 MBq/kg body weight) (Bodei, 2008). Onset of pain relief comes within one week, lasting from four weeks up to four months. The highest absorbed dose is received by bone marrow and bone surfaces. Imaging is commonly performed three hours after injection to verify the activity uptake. All activity not taken up in bone is excreted via urine and no further activity is excreted 24 hours after the injection. Dosimetry can therefore be performed from one scintillation camera imaging acquired 24h after injection or from one single probe measurement. The activity uptake in bone has been reported to increase with an increase in number of bone tumors (Farhangi, 1992; Brenner, 2001).

Renium-186 is a beta minus emitter with a maximum beta energy of 1.07 MeV. The physical half-life is 89 hours. The radiopharmaceutical is taken up in bone via the phosphor complex HEDP (hydroxyethylidene diphosphonate). Quantitative imaging for pharmacokinetics and dosimetry is possible via the emission of 137 keV photons with a 9.47% probability. Excretion is predominantly through the kidneys.

Radium-223-chloride is taken up in bone by natural affinity. It decays in six steps into stable ^{207}Pb. The injected activity has been reported as 46-250 kBq per kg of whole body weight (Nilsson, 2005, 2007). A clinical phase II study showed an improved survival without severe toxicity after four weekly injections of 50 kBq per kg of whole body weight compared to placebo injections (Nilsson, 2007). The photon emissions at 81.1 keV and 83.8 keV show the highest emission probabilities and offer the best opportunity to perform quantitative imaging during the treatment, which enables pharmacokinetic and dosimetric studies to be performed. The main route of excretion is via faeces (Hindorf, 2008).

Contraindications for radionuclide therapy are a life expectancy shorter than four weeks, severe renal insufficiency, and low blood counts due to a compromised bone marrow function. The absorbed dose to the tumour is the factor that determines the effectiveness of the therapy while the absorbed dose to the bone marrow correlates to the toxic effects received. The bone marrow is the dose limiting organ when bone-seeking radiopharmaceuticals are used (Lewington, 1993). Radionuclide therapy for pain palliation from bone metastases is currently performed based on a pre-set injected activity. The patients will, therefore, receive a range of absorbed doses due to individual differences in the pharmacokinetics. Voxel based, patient specific dosimetry automatically takes into account individual differences in pharmacokinetics and macroscopic anatomy. Furthermore, Monte Carlo simulations also take into account different cross sectional interaction data for all materials present in the body, which is, therefore, more accurate than convolution with a dose point kernel as this is based on an assumption of infinite, uniform medium.

Radionuclide therapy as a palliative treatment of bone pain is efficient, although improved dosimetry methods could help to improve the treatment further.

10. Peptide radio-receptor therapy of neuroendocrine tumours

Neuroendocrine tumours (NETs) derive from the neuroendocrine cell system, which is widely distributed in the body, and are a heterogeneous group of neoplasms characterized by embryological, biological and histo-pathological differences. The most frequent sites of NETs are the gastrointestinal tract (70%) and the bronco-pulmonary system (25%), followed by the skin, the adrenal glands, the thyroid and the genital tract.

Present classification is based on tumour biology and patho-histological features (cellular grading, primary tumour size and site, cell proliferation markers, local or vascular invasivity and the production of biologically active substances), which are crucial to guide the diagnostic work-up and therapeutic planning.

The great majority are benign (well-differentiated neuroendocrine tumours) or slow-growing neoplasms with a low grade of malignancy. Poorly differentiated endocrine carcinomas have a high grade of malignancy and a poor prognosis. Furthermore, a few moderately differentiated tumours with cellular and structural types intermediate between well and poorly differentiated NETs have also been found.

A typical feature of differentiated NETs is the expression of several specific receptors on the cell membrane and in particular of somatostatin receptors (SSTR) which can be visualized by somatostatin receptor imaging with radiolabelled somatostatin analogues (^{111}In-OCTREOSCAN, ^{68}Ga-DOTANOC). These radiopharmaceuticals bind with high affinity to subtypes 2, 5 and 3 of SSTR and provide an approximation of somatostatin receptor density, having a positive predictive value of the therapeutic efficacy of the somatostatin analogues.

Peptide receptor radionuclide therapy (PRRT) is an effective tool for the treatment of tumours with a high somatostatin receptor density.

This approach is based on the administration of a therapeutic activity of radiolabelled somatostatin analogues. Radiopharmaceutical with various radionuclides and peptides are currently available.

High activities of ^{111}In-DTPA-octreotide (OCTREOSCAN®), the same radiopharmaceutical used for imaging, have been used in pilot trials and in some experiences (Herberg, 2009, 2011). Besides the gamma radiation of ^{111}In used for scintigraphic scans (γ photons of 172 and 245 keV), its therapeutic effect is due to the emission of Auger and conversion electrons with a medium-to-short tissue penetration range (0.02-10 and 200-500 μm, respectively). Its potential effect depends on the preservation of mechanism of octreotide-receptor complex internalization (through endocytosis) and its translocation to the nuclear compartment, where short path-length Auger or conversion electrons are able to reach the target (DNA). In clinical trials, ^{111}In-DTPA-octreotide showed a low rate of tumour regression: the most accredited explanation is that ^{111}In electrons fail to reach the DNA helix, possibly due to the lack of nuclear receptors that were never definitely demonstrated (Kwekkeboom, 2005).

The radiopeptides for PRRT that have been studied most extensively are ^{90}Y-DOTATOC and ^{177}Lu-DOTATATE. These beta-emitting radiolabelled peptides are preferred for their advantageous physical properties.

^{90}Y (E_{max} = 2.28 MeV, R_{max} = 11 mm, <E> = 0.935 MeV; half-life 2.67 days) has a pure beta emission with long range particles that, besides the direct action, lead to irradiation also of no-receptor expressing tumour-cell (cross-fire effect). For these reasons ^{90}Y-peptides are

preferred especially for the treatment of larger and inhomogeneous lesions. In figure 5, the comparison between electron paths within small and large inhomogeneous lesions is represented through a Monte Carlo simulation in Geant4, in which radiations emitted from ^{177}Lu and ^{90}Y are compared.
^{177}Lu has a longer half-life (6.7 days) and lower energy beta-emission (E_{max} = 0.497 MeV; R_{max} = 2 mm) that allows to concentrate all the energy inside smaller tumours; moreover the gamma-emission of ^{177}Lu (113 keV and 208 keV) is suitable for scintigraphy and dosimetry during PRRT.

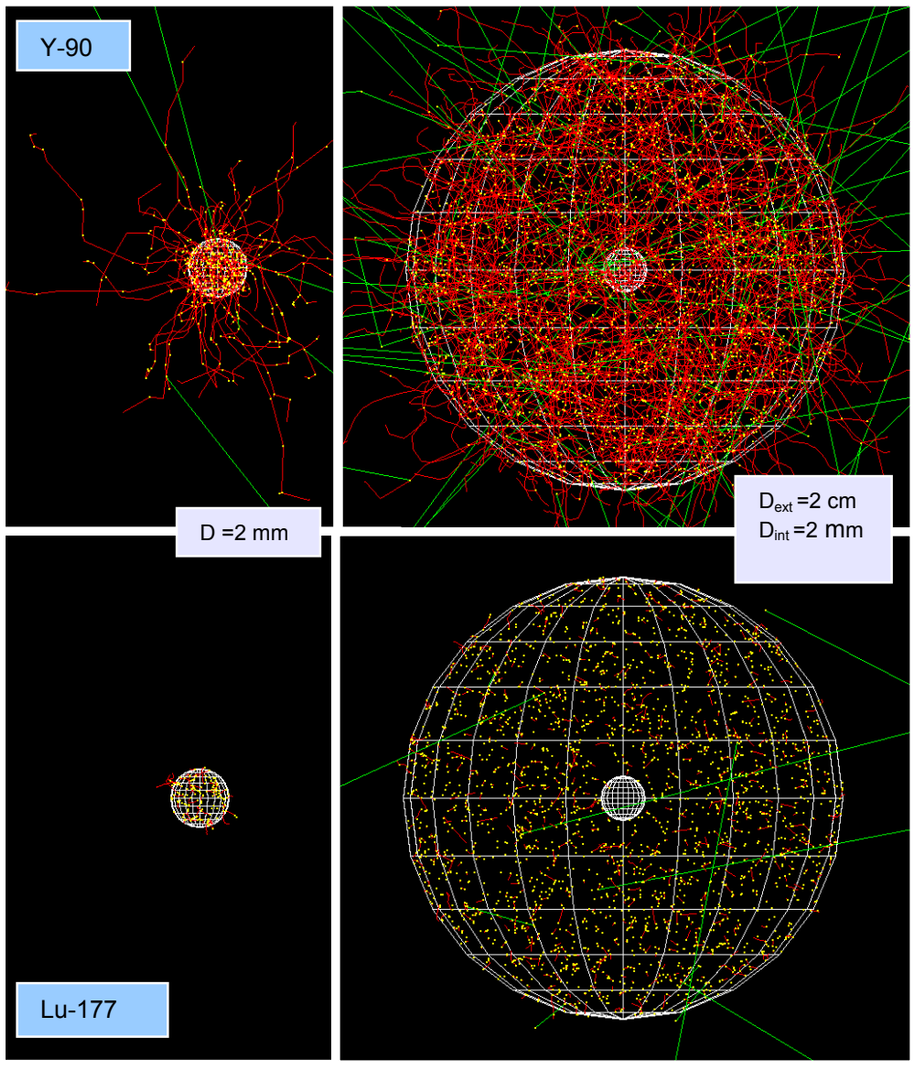

Fig. 5. Comparison between the high-energy electron tracks (red) of ^{90}Y and the ones of the lower-energy electrons from ^{177}Lu. Photons originating from gamma ray emission or bremsstrahlung are represented in green.

Concerning peptides, several new somatostatin analogues have been introduced for therapeutic and diagnostic purposes, including the agonists DOTA-(1-NaI3)octreotide (DOTANOC) and DOTA-(BzThi3)octreotide (DOTABOC).

These compounds have a broader somatostatin receptor affinity profile than DOTATATE and DOTATOC because of a higher affinity for sst3 and sst5 in addition to their high affinity for sst2. This could increase the number of tumours that could benefit from PRRT in the future.

Recently, peptides targeting all the sst receptors (pansomatostatins) have shown high affinity of ^{90}Y-DOTA-cyclo(D-diaminobutyric acid-Arg–Phe–Phe-D-Trp–Lys–Thr–Phe) (^{90}Y-KE88) for all 5 sst receptors and, in future, they could improve the therapeutic potential of sst-targeted PRRT.

To date, the therapy administration protocols rely essentially on empirical criteria with injection of standard activities, as derived from escalation studies or clinical experience, at variable time intervals (6-12 weeks).

For therapy optimization and prevention of toxicity, dosimetry represent a precious guide, providing evaluation of biodistribution, pharmacokinetics, radiation doses and biological effective doses to healthy organs and tumours.

The gamma-emission of ^{111}In and ^{177}Lu-peptide enable imaging, dosimetry and therapy with the same compound. In the case of ^{90}Y-peptide, for the lack of gamma emission, the same analogue radiolabeled with ^{111}In or positron emitters as ^{86}Y or ^{68}Ga can be used as surrogates for dosimetric imaging. Some recent studies have been published for ^{90}Y-peptide dosimetry with bremsstrahlung images through SPECT-TC systems, or exploiting the rare positron decay of ^{90}Y imaged by new generation PET-CT scanners.

A dosimetric protocol consists in the acquisition of multiple planar whole-body (WB) scan to obtain biokinetics data over the time (at least 4-5 acquisitions at different times), complementary SPECT imaging to evaluate intra-organ activity distribution (especially at the level of the kidneys and in tumour lesion), WB transmission imaging for attenuation correction, blood and urine samples. Anatomical imaging (CT or ultrasonographic) provide important parameters for organ mass evaluation (Cremonesi, 2011).

Dose calculation can be performed in the framework of the MIRD formalism, in order to obtain average dose estimates at the organ level assuming standard phantom models, with possible organ mass adjustments according to patient data. Voxel dosimetry method or direct Monte Carlo simulation can provide more reliable dose estimates.

Pharmacokinetic studies have shown fast blood clearance and urinary elimination. The higher uptake has been noticed in the spleen, kidneys and liver and no uptake is visible in the bone marrow in normal conditions. Pharmacokinetic data of different radiopeptides are similar but not identical: as the peptide influences biokinetics, for the single patient the data need to be assessed specifically with regard to the radiopharmaceutical.

Furthermore, dosimetric data should be collected during therapeutic cycles because many factors can influence the results.

The adsorbed doses, especially with regards to the tumour, are affected by wide intra-patient variation between treatment cycles. The adsorbed dose to the tumour is higher during the first two cycles with a gradually reduced uptake in the following treatments, probably due to saturation or down-regulation of peptide receptors. Tumour adsorbed dose should exceed 100 Gy to obtain a therapeutic effect, with better results for higher doses (about 230 Gy).

Nephrotoxicity is the dose-limiting factor, due to renal reabsorption and retention of radiolabeled peptides that results in high kidney radiation doses.

The renal adsorbed dose is influenced by the radionuclide emission: using a microdosimetry model, Konijnenberg et al. (2004) found that ^{111}In- and ^{177}Lu-labelled somatostatin analogues

are likely to have higher renal toxicity thresholds than ^{90}Y, whose emitted electrons have a path length of 12 mm.
Renal doses can be reduced by co-administration of basic amino acids, bovine gelatine-containing solution Gelofusine or albumin fragments, which interfere with the radiopeptide reabsorption pathway to achieve kidney protection. Amino acids, in particular, are already commonly used in the clinical setting during PRRT, being able to reduce the kidney adsorbed dose consistently (25-65% with respect to baseline data). The dose fraction markedly influences the total tolerated dose.
The dose to kidneys should not exceed a limit value of 28 Gy, established for external beam radiotherapy, which results in a 50% probability of developing severe late renal failure. Nevertheless, for the difference between the two radiation therapy modalities, this recommendation has been questioned and the biological effective dose (BED) is considered a more accurate quantity, with a good correlation with the loss of kidney function.
BED for a given organ or tissue was defined in Equation 18. We recall that BED is a function of the doses imparted in each PRRT cycle, and depends upon the effective half-time of the radiopeptide in the organ and upon its intrinsic radiosensitivity.
Data in literature show that patients with risk factors, such as hypertension and diabetes, should not receive a BED higher than 28 Gy, while patients with no risk factors might have a renal BED threshold of 40 Gy (Bodei, 2008).
The risk of bone marrow toxicity increases with increasing therapeutic dose. Studies aimed to increase the therapeutic dose (more cycles, higher dose per cycle, improvement in specific activity of the compound) to the tumour in a renoprotective (and bone marrow-protective) regimen are needed to further improve PRRT with somatostatin analogues in the future.

11. References

Amato, E. et al. (2009). Absorbed fractions for photons in ellipsoidal volumes. *Phys Med Biol,* 54, N479-487.

Amato, E. et al. (2009). Absorbed fractions in ellipsoidal volumes for β− radionuclides employed in internal radiotherapy. *Phys Med Biol,* 54, 4171-4180.

Amato, E. et al. (2011). Absorbed fractions for electrons in ellipsoidal volumes. *Phys Med Biol,* 56, 357-365.

Amato, E. et al. (2011). An analytical model for improving absorbed dose calculation accuracy in non spherical autonomous functioning thyroid nodule. *Quart. J. Nucl. Med. Mol. Imag.* EPUB 18-01-2011 PMID: 21242948.

Berenson, J. R. (2005). Recomendations for zoledronic acid treatment of patients with bone metastases. *Oncologist,* 10, 52-62.

Blake, G. et al. (1998). Strontium-89 therapy: measurements of absorbed dose to skeletal metastases. *J Nucl Med,* 29, 549-557.

Blake, G. M. et al. (1986). Sr-89 therapy: strontium kinetics in disseminated carcinoma of the prostate. *Eur J Nucl Med,* 12, 447-454.

Blake, G. M. et al. (1987). 89Sr radionuclide therapy: dosimetry and haematological toxicity in two patients with metastasising prostatic carcinoma. *Eur J Nucl Med,* 13, 41-46.

Bodei, L. et al. (2008). Long-term evaluation of renal toxicity after peptide receptor radionuclide therapy with 90Y-DOTATOC and 177Lu-DOTATATE: the role of associated risk factors. *Eur. J. Nucl. Med.* 35, 1847.

Bodei, L. et al. (2008). EANM procedure guideline for treatment of refractory metastatic bone pain. *Eur J Nucl Med Mol Imaging,* 35, 1934-1940.

Bolch, W.E. et al. MIRD Pamphlet No. 17: the dosimetry of nonuniform activity distributions – radionuclide S values at the voxel level. *J Nucl Med,* 40, 11S-36S.

Breen, S. L. et al. (1992). Dose estimation in strontium-89 radiotherapy of metastatic prostatic carcinoma. *J Nucl Med,* 33, 1316-1323.

Brenner, W. et al. (2001). Skeletal uptake and soft-tissue retention of 186Re-HEDP and 153Sm-EDTMP in patients with metastatic bone disease. *J Nucl Med,* 42, 230-236.

Cremonesi, M. et al. (2011). Recent issues on dosimetry and radiobiology for peptide receptor radionuclide therapy. *Quart. J. Nucl. Med. Mol. Imag,* 55(2), 155-167.

Dafermou, A. et al. (2001). A multicentre observational study of radionuclide therapy in patients with painful bone metastases of prostate cancer. *Eur J Nucl Med Mol Imaging,* 28, 788-798.

Dieudonnè, A. et al. (2010). Fine-resolution voxel S values for constructing absorbed dose distributions at variable voxel size. *J Nucl Med,* 51, 1600-1607.

Englaro, E.E. et al. (1992). Safety and efficacy of repeated sequential administrations of Re186(Sn)HEDP as palliative therapy for painful skeletal metastases. Initial case reports of two patients. *Clin Nucl Med,* 17, 41-44.

Eschmann, S. M. et al. (2002). Evaluation of dosimetry of radioiodine therapy in benign and malignant thyroid disorders by means of iodine-124 and PET. *Eur. J. Nucl. Med. Mol. Imaging,* 29, 760-767.

Farhangi, M. et al. (1992). Samarium-153-EDTMP: pharmacokinetic, toxicity and pain response using escalation doses schedule in treatment of metastatic bone cancer. *J Nucl Med,* 33, 1451-1458.

Furhang, E. E. et al. (1997). Implementation of a Monte Carlo dosimetry method for patient-specific internal emitter therapy. *Med. Phys,* 24, 1163-1172.

Giovannella (2000). *Radiol. Med.*, 105, 12

Hellmann, S. and Weichsellbaum, R. R. (1994). Radiation oncology. *JAMA*, 271, 1712-1714.

Herberg, A. et al. (2009). 90Y-DOTATOC and/or 111In-Pentetreotide in the treatment of somatostatin receptors-expressing tumors (SSTR): our experience. *Eur J Nucl Med Mol Imaging*, 36 S.2, S418.

Herberg, A. et al. (2011). 111In-Pentetreotide for the treatment of neuroendocrine tumours: an alternative therapeutic option in particular cases. *Quart J Nucl Med Mol Imaging*, 52 S.1, 131.

Hillner, B.E. et al. (2003). American Society of Clinical Oncology 2003 update on the role of bisphosphonates and bone health issues in women with breast cancer. *J Clin Oncol,* 21, 4042-4057.

Hindorf, C. et al. (2008). A biodistribution and dosimetry study of therapeutic 223RA-chloride (Alpharadin) in patientts with osteoblastic skeletal metastases secondary to hormone refractory prostate cancer. *J Nucl Med,* 49, 145P.

Hindorf, C. et al. (2008). Quantitative imaging of 223Ra during radionuclide therapy of bone metastases. *J Nucl Med,* 49, 326P.

Hindorf, C. et al. (2011). Clinical dosimetry in the treatment of bone tumors: old and new agents. *Q J Nucl Med Mol Imaging,* 55, 198-204.

ICRP, (1987). International Commission on Radiological Protection. Radiation dose to patients from radiopharmaceuticals. Oxford, UK; Pergamon Press.

Konijnenberg, M. W. et al. (2004). A stylized computational model of the rat for organ dosimetry in support of preclinical evaluations of peptide receptor radionuclide therapy with (90)Y, (111)In, or (177)Lu. *J Nucl Med,* 45, 1260–1269.

Kraeber-Bodere, F. et al. (2000). Treatment of bone metastases of prostate cancer with strontium-89chloride: efficacy in relation to degree of bone involvement. *Eur J Nucl Med* 27, 1487-1493.

Krishnamurthy, G. T. et al. (1997). Tin-117m(4+)DTPA: pharmacokinetics and imaging characteristics in patients with metastatic bone pain. *J Nucl Med,* 38, 230-237.

Krishnamurthy, G. T. et al. (2000). Radionuclides for metastatic bone pain palliation:a need for rational re-evaluation in the new millenium. *J Nucl Med,* 41, 688-691.

Kwekkeboom, D. J. et al. (2005).
Overview of Results of Peptide Receptor Radionuclide Therapy with 3 Radiolabeled Somatostatin Analogs
. *J. Nucl. Med.* 46, 62S.

Lam, M. J. E. H. et al. (2004). 186Re-HEDP for metastatic bone pain in breast cancer patients. *Eur J Nucl Med Mol Imaging,* 31, S162-S170.

Lassmann, M. (2010). *Dosimetry Concepts of radioiodine therapy for the Treatment of differentiated thyroid cancer,* EANM Dosimetry Committee

Leondi, A. H. et al. (2004). Palliative treatment of painful disseminated bone metastases with 186Rhenium-HEDP in patients with lung cancer. *Q J Nucl Med,* 48, 211-219.

Lewington, V. J. (1993). Targeted radionuclide therapy for bone metastases. *Eur J Nucl Med,* 20, 66-74.

Lewington, V. J. (2005). Bone-seeking radionuclides for therapy. *J Nucl Med,* 46, 38S-47S.

Lewington, V.J. (1996). Cancer therapy using bone-seeking isotopes. *Phys Med Biol,* 41, 2027-2042.

Maigne, L. et al. (2011). Comparison of GATE/GEANT4 with EGSnrc and MCNP for electron dose calculations at energies between 15 keV and 20 MeV. *Phys. Med. Biol,* 56, 811.

Mainegra-Hing, E. et al. (2005). Calculation of photon energy deposition kernels and electron dose point kernels in water. *Med. Phys,* 32, 685-699.

Maini, C. L. et al. (2003). Radionuclide therapy with bone seeking radionuclides in palliation of painful bone metastases. *J Exp Clin Cancer Res,* 22, 71-74.

Maini, C. L. et al. (2004). 153Sm-EDTMP for bone pain palliation in skeletal metastases. *Eur J Nucl Med Mol Imaging,* 31, S171-S178.

Mazzaferri E. L. (1997). Thyroid Remnant 131I Ablation for Papillary and Follicular Thyroid Carcinoma. *Thyroid,* 7, 265271.

Minutoli, F. et al. (2006). 186Re-HEDP in the palliation of painful bone metastases from cancers other than prostate and breast. *Q J Nucl Med*, 50, 355-362.

Nilsson, S. et al. (2005). First clinical experience with alpha-emitting radium-223 in the treatment of skeletal metastases. *Clin Cancer Res*, 11, 4451-4459.

Nilsson, S. et al. (2007). Bone-targeted radium-223 in symptomatic, hormone-refractory prostate cancer: a randomised, multicentre, placebo-controlled phase II study. *Lancet Oncology,* 8, 587-594.

Regalbuto, C. et al. (2009). Radiometabolic treatment of hyperthyroidism with a calculated dose of 131-iodine: results of one-year follow-up. *J. Endocrinol. Invest,* 32, 134-138.

Roche, E. and Prentky, M. (1994). Calcium regulation of immediate early responce genes. *Cell Calcium*, 16, 331-338.

Sgouros, G. et al. (2004). Patient-Specific Dosimetry for 131I Thyroid Cancer Therapy Using 124I PET and 3-Dimensional-Internal Dosimetry (3D-ID) Software. *J. Nucl. Med,* 45, 1366-1372.

Silberstein, E. B. (2001). Painful osteoblastic metastases: the role of nuclear medicine. *Oncology,* 15, 157-163.

Snyder, W. et al. (1975). "S" absorbed dose per unit cumulated activity for selected radionuclides and organs MIRD Pamphlet No. 11. New York (NY): Society of Nuclear Medicine.

Srivastava, S. C. et al. (1998). Treatment of metastatic bone pain with tin-117m stannic diethylenetriaminepentaacetic acid: a phase I/II clinical study. *Clin Cancer Res,* 4, 61-68.

Strigari, L. et al. (2011). Dosimetry in nuclear medicine therapy: radiobiology application and results. *Quart. J. Nucl. Med. Mol. Imag,* 55(2), 205-221.

Tennvall, J. et al. (1988). Palliation of multiple bone metastases from prostatic carcinoma with strontium-89. *Acta oncologica,* 27, 365-369.

IntechOpen

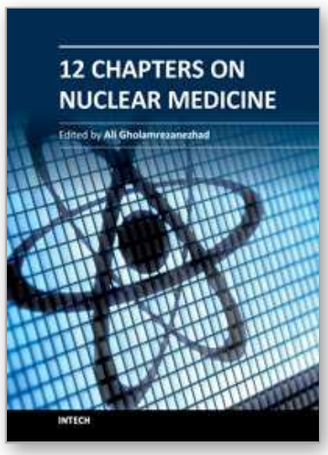

12 Chapters on Nuclear Medicine

Edited by Dr. Ali Gholamrezanezhad

ISBN 978-953-307-802-1

Hard cover, 304 pages

Publisher InTech

Published online 22, December, 2011

Published in print edition December, 2011

The development of nuclear medicine as a medical specialty has resulted in the large-scale application of its effective imaging methods in everyday practice as a primary method of diagnosis. The introduction of positron-emitting tracers (PET) has represented another fundamental leap forward in the ability of nuclear medicine to exert a profound impact on patient management, while the ability to produce radioisotopes of different elements initiated a variety of tracer studies in biology and medicine, facilitating enhanced interactions of nuclear medicine specialists and specialists in other disciplines. At present, nuclear medicine is an essential part of diagnosis of many diseases, particularly in cardiologic, nephrologic and oncologic applications and it is well-established in its therapeutic approaches, notably in the treatment of thyroid cancers. Data from official sources of different countries confirm that more than 10-15 percent of expenditures on clinical imaging studies are spent on nuclear medicine procedures.

How to reference

In order to correctly reference this scholarly work, feel free to copy and paste the following:

Ernesto Amato, Alfredo Campennì, Astrid Herberg, Fabio Minutoli and Sergio Baldari (2011). Internal Radiation Dosimetry: Models and Applications, 12 Chapters on Nuclear Medicine, Dr. Ali Gholamrezanezhad (Ed.), ISBN: 978-953-307-802-1, InTech, Available from: http://www.intechopen.com/books/12-chapters-on-nuclear-medicine/internal-radiation-dosimetry-models-and-applications

INTECH
open science | open minds

InTech Europe
University Campus STeP Ri
Slavka Krautzeka 83/A
51000 Rijeka, Croatia
Phone: +385 (51) 770 447
Fax: +385 (51) 686 166
www.intechopen.com

InTech China
Unit 405, Office Block, Hotel Equatorial Shanghai
No.65, Yan An Road (West), Shanghai, 200040, China
中国上海市延安西路65号上海国际贵都大饭店办公楼405单元
Phone: +86-21-62489820
Fax: +86-21-62489821

© 2011 The Author(s). Licensee IntechOpen. This is an open access article distributed under the terms of the Creative Commons Attribution 3.0 License, which permits unrestricted use, distribution, and reproduction in any medium, provided the original work is properly cited.

IntechOpen

IntechOpen